Cross-diagnostic analysis of plasma filaments on the Wendelstein 7-X stellarator

A. Buzás[1,2], G. Anda[1], C. Biedermann[3], G. Cseh[1], B. Csillag[1], D. Dunai[1], G. Kocsis[1], M. Krause[3], D. Nagy[1], M. Otte[3], D. Réfy[1], T. Szepesi[1], M. Vécsei[3], S. Zoletnik[1], and the W7-X Team *

[1] *HUN-REN Centre for Energy Research, Budapest, Hungary*

[2] *Institute of Nuclear Techniques, BME, Budapest, Hungary*

[3] *Max-Planck-Institute for Plasma Physics, Greifswald, Germany*

Plasma filaments are a common feature of the edge plasma in toroidal fusion devices. They are field-aligned density perturbations linked to the interchange instability caused by the steep edge profiles, propagated by ExB drift [1]. Unlike in tokamaks, recent studies [2, 3] argue that their contribution to cross-field transport across the SOL is less significant on W7-X, instead their importance lies in setting the density profiles of the magnetic islands [4]. In the complex magnetic geometry of W7-X, the usual 2D description of filaments is insufficient. Their behavior also varies depending on the magnetic configuration [4, 5]. Fast cameras provide an excellent tool for studying that complex, 3D structure, however, they are limited by the width of the radiation belt. This shortcoming can be compensated by including other diagnostics in the analysis. Alkali beam emission spectroscopy (ABES), for example, has excellent radial resolution across the SOL, mid-plane island, and edge. In this study, a joint analysis of fast camera and ABES data is presented. By correlating the two diagnostics, the toroidal structure, and poloidal and radial movement of the filaments are observed in the W7-X standard magnetic configuration.

To investigate filament activity, the W7-X fast camera system [6] and the ABES diagnostics were used. ABES is based on injecting a neutral sodium beam into the plasma. As the neutral atoms collide with plasma electrons, they get excited and emit light while returning to their ground state. This light is roughly proportional to the local plasma density and is measured by APD cameras. [3] In standard configuration, the beam crosses the o-point of the island at the equatorial plane. Figure 1 shows the radial positions of the observation points of the ABES channels. Figure 2 shows the projections of the field lines connecting the camera view with the ABES channels in both toroidal directions. For analyzing visible emissions, a Photron fast camera was used. It is located at port AEA21. While the camera view covers the entire

* See Pedersen et al 2021 (https://doi.org/10.1088/1741-4326/ac2cf5) for the W7-X Team.

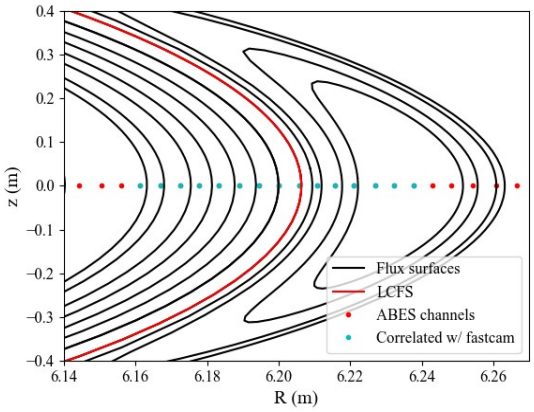

Figure 1: Radial positions of the ABES observation points. Blue ones correlate with the fast camera images. Flux surfaces of standard configuration are drawn for visual reference.

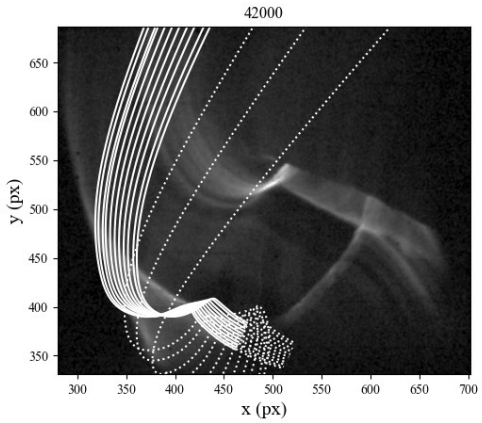

Figure 2: Projection of field lines connecting the camera view with the ABES channels in both toroidal directions (solid line forward, dotted backward).

poloidal cross-section of the plasma, its radial observations are limited to a visible radiation belt a few cm wide. For this analysis, the camera was equipped with a 465 nm interference filter which is the C III emission line. C^{2+} ions are major contributors to the light of the radiation belt. For more detail, please refer to [5].

In this contribution, the results from shot 20230323.044 are presented. It is a standard configuration shot recorded at 40 kHz. The images were binned (averaged over 3x3 grids to reduce noise) and filtered between 2 and 11 kHz, which is typical for filament activity. Pixelwise correlations are then calculated. Reference points are usually selected on the projection of a flux surface at a given toroidal angle so they can be matched to points of known 3D coordinates. For more detail, see [5]. Figure 3 shows the maximal correlation of each pixel to the reference point indicated by a green star. Figure 4 shows the corresponding time delay. Here, the succession of colors (from blue to red) indicates the direction of movement. In this image, the movement of filaments is clockwise, which in this view corresponds to a negative E_r, which is typical in the edge for similar shots. [7] Their poloidal velocity is estimated to be around 1.2 km/s, which agrees well with earlier results. [2, 5] Based on the correlation patterns, it is apparent that filaments loop around the device toroidally at least once. The multiple correlated lines in these images are caused by separate events, each looping around, projected over the same pixel.

The APDCAM was operating at 2 MHz, and the beam was chopped out of the plasma at 200 kHz. Averaging over the segments when the beam was on and subtracting the background gives a signal of 100 kHz, which is filtered between 2 and 10 kHz. Correlations between the

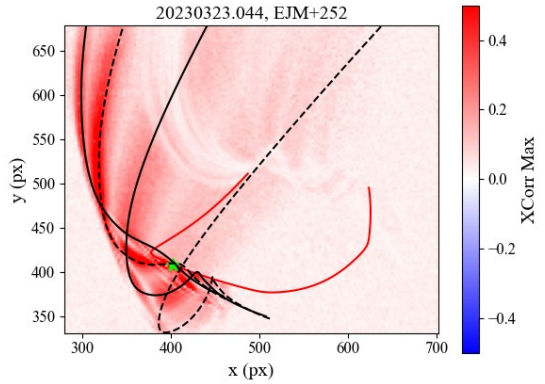

Figure 3: Max correlation to a reference point (green star). The red curve is the projected flux surface from which the reference point is chosen. Black lines are field lines whose projections cross the reference point.

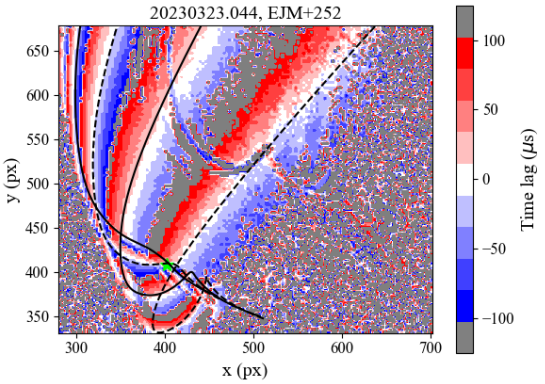

Figure 4: Time delays belonging to figure 5. Colors indicate toroidal turnaround of filaments and clockwise movement. Separate but not connected events projected over the same region (solid and dashed lines).

channels provide insight into the radial movements of filaments. For this shot, meaningful information can only be gained from the SOL. In the edge, the signal is dominated by the shadows of SOL filaments caused by beam loss due to ionization (see the negative correlation with 0 time lag inside the LCFS in both figure 5 and 6). After the LCFS, the correlated area is about 1.8 cm wide (figure 5). There is no time delay for the correlation maxima, so if there is radial movement, it must be faster than 500 m/s. There is anti-correlation on both sides of this region, meaning that it is affected but not dominated by the shadow of filaments further out. Closer to the o-point (figure 6), there are clear signs of radial motion of about 200 m/s. In the far SOL, there is no correlation between the channels.

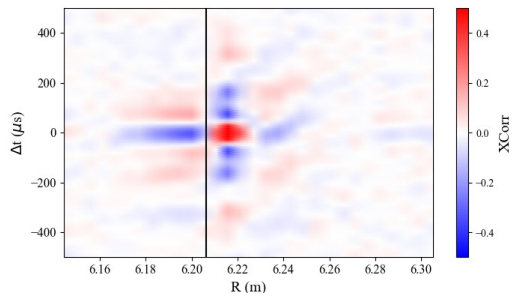

Figure 5: Correlation between ABES channels. Reference 1 cm outside the LCFS (vertical lines).

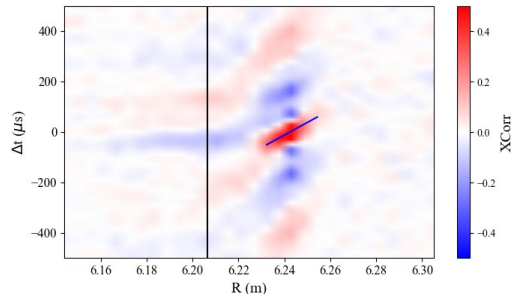

Figure 6: Here, the reference is close to the o-point. The tilted line is fitted to the correlation maxima.

There is a strong correlation between the two diagnostics over multiple channels on both sides of the LCFS. Figure 7 shows the time delay of the maximal correlation with a channel 1 cm outside the LCFS, while figure 8 shows a channel 1 cm inside. The reversed succession of colors between the two figures indicates poloidal movement in the opposite directions, which

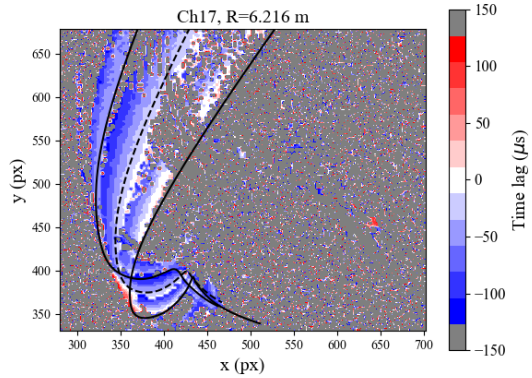

Figure 7: Time delay of max correlation between the near SOL and the camera images. Solid lines connect the reference channel and the camera view. The dashed line is a different field line on the LCFS.

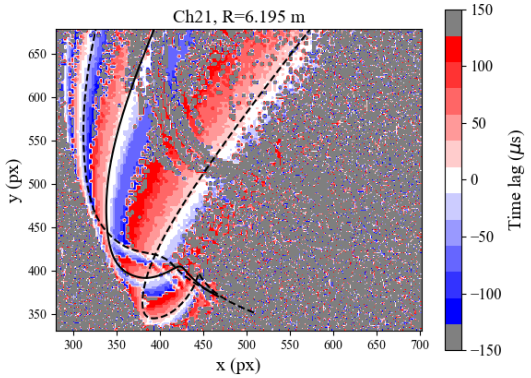

Figure 8: Time delay of the correlation between the edge and the camera. The solid line connects the reference channel with the camera view. The dashed lines are different field lines.

is consistent with the expected sign change of E_r around the LCFS. [7] The lack of positive time delay in figure 7 can be interpreted by either the observed structures leaving the radiation belt or decorrelating right after crossing the beam. The time lag along their path is consistent with the typical lifetime of filaments [5]. Interestingly, correlation appears not only over the field lines that connect the ABES channels with the camera view (solid lines in figure 7-8), but over others too (dashed lines). Theory suggests that alongside filaments, reduced density structures (holes) form as well, moving radially inwards [1]. If such structures appear on the camera images, they may correlate positively with the shadows of filaments radially further out. However, this is only an assumption yet and requires further investigation. Based on the radial distance of the correlated channels and the width of the correlation between them, a rough estimate of about 5 cm can be given for the width of the radiation belt.*

References

[1] D'Ippolito D. A. et al Phys. Plasmas 18, 060501 (2011)

[2] Killer C. et al Plasma Phys. Control. Fusion 62, 085003 (2020)

[3] Zoletnik S. et al Plasma Phys. Control. Fusion 62, 014017 (2020)

[4] Csillag B. et al Nucl. Fusion 64, 016017, (2020)

[5] Buzas A. et al Nucl. Fusion 64, 066012, (2020)

[6] Kocsis G. et al Fus. Eng. Des. 96-97, 808, (2015)

[7] Carralero D. et al Nucl. Fusion 60, 106019, (2020)

* This work has been carried out within the framework of the EUROfusion Consortium, funded by the European Union via the Euratom Research and Training Programme (Grant Agreement No 101052200 — EUROfusion). Views and opinions expressed are however those of the author(s) only and do not necessarily reflect those of the European Union or the European Commission. Neither the European Union nor the European Commission can be held responsible for them.